Heliyon 10 (2024) e27193

Contents lists available at ScienceDirect

Heliyon

journal homepage: www.cell.com/heliyon

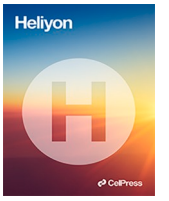

Research article

Unraveling the binding mechanisms of SARS-CoV-2 variants through molecular simulations

Shin-Pon Ju [a,b,*], Yung-Cheng Yang [a], Hsing-Yin Chen [b]

[a] Department of Mechanical and Electro-Mechanical Engineering, National Sun Yat-sen University, Kaohsiung 804, Taiwan
[b] Department of Medicinal and Applied Chemistry, Kaohsiung Medical University, Kaohsiung 807, Taiwan

ARTICLE INFO

Keywords:
SARS-CoV-2
Spike protein
Variants
Coare-grained molecular dynamics
Binding affinity
ACE2 receptor

ABSTRACT

The emergence of SARS-CoV-2 variants like Delta (AY.29) and Omicron (EG.5) poses continued challenges for vaccines and therapeutics. Mutations in the viral spike protein are key in altering infectivity and immune evasion. This study uses computational modeling to investigate the molecular binding mechanisms between spike protein variants and the ACE2 host receptor. Using the MARTNI force field, coarse-grained molecular dynamics (CGMD) simulations and nudged elastic band (NEB) calculations explore spike-ACE2 interactions for the wild type, Delta variant, and Omicron variant. The simulations reveal Omicron has the strongest binding affinity at −128.35 ± 10.91 kcal/mol, followed by Delta and wild type. Key mutations in Delta and Omicron, like Q493R and Q498R, optimize electrostatic contacts, enhancing ACE2 interactions. The wild-type spike has the highest transition state energy barrier at 17.87 kcal/mol, while Delta has the lowest barrier at 9.21 kcal/mol. Despite slightly higher dual barriers, Omicron's increased binding energy lowers its overall barrier to rapidly bind ACE2. These findings provide residue-level insights into mutation effects on SARS-CoV-2 infectivity. The computational modeling elucidates mechanisms underlying spike-ACE2 binding kinetics, aiding the development of vaccines and therapies targeting emerging viral strains.

1. Introduction

Coronavirus disease 2019 (COVID-19) was declared a global pandemic in March 2020, resulting in millions of fatalities and profound impacts on health, society, and the economy [1]. Administering COVID-19 vaccines effectively reduces mortality; however, the emergence of COVID-19 variants might influence antibody-mediated vaccine recognition [2]. S1 recognizes host receptors, primarily angiotensin-converting enzyme-2 (ACE2). Cells initially insensitive to SARS-CoV-2 become susceptible upon ACE2 transfection [2]. Recombinant ACE2 reduces early SARS-CoV-2 infection and safeguards human kidney organoids. Wang et al. created ACE2-bearing membrane nanoparticles (NPs) [3]. These ACE2-NPs acted as S1 traps, hindering viral ligand recruitment to human renal tubular cells. ACE2-NPs counteracted S1-induced apoptosis. They effectively obstructed SARS-CoV-2 pseudovirions from entering host cells in vitro and in vivo. Tsai's study revealed GB-1, developed from the Chiehyuan herbal formula, inhibits ACE2 binding to various SARS-CoV-2 variants [4]. Glycyrrhizic acid from GB-1 obstructs ACE2-RBD interaction, curtailing SARS-CoV-2 transmission. These findings align with Li's work [5], showing glycyrrhizic acid's interference with spike protein-cell interactions.

* Corresponding author. Department of Mechanical and Electro-Mechanical Engineering, National Sun Yat-sen University, Kaohsiung 804, Taiwan.
E-mail address: jushin-pon@mail.nsysu.edu.tw (S.-P. Ju).

https://doi.org/10.1016/j.heliyon.2024.e27193
Received 26 September 2023; Received in revised form 25 February 2024; Accepted 26 February 2024
Available online 29 February 2024

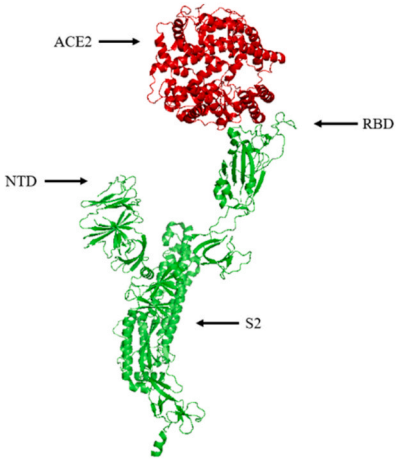

(a)

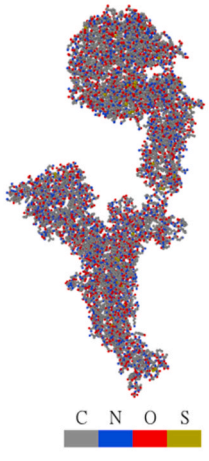

(b)

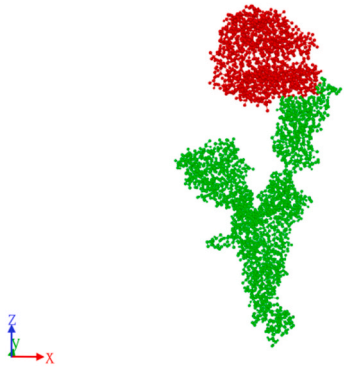

(c)

(caption on next page)

Fig. 1. The wild type SARS-CoV-2 spike protein and ACE2 complex in (a) the ribbon model (the red and green parts highlight ACE2 and spike protein, respectively), (b) the corresponding all-atom model with a total of 13677 atoms (color-coded according to their corresponding element types, namely, C, N, O, and S.), and (c) the corresponding coarse-grained model for MARTINI force field (the red and green parts highlight ACE2 and spike protein, respectively).

Wei et al. demonstrated chicken egg yolk antibodies (IgYs) hinder multiple spike protein variants from interacting with ACE2 [6]. IgYs neutralized SARS-CoV-2 pseudovirus, including different spike protein mutants. These experimental studies underscore molecular recognition's potential in innovative SARS-CoV-2 therapeutic strategies. ACE2-NPs, GB-1, and IgYs impede virus-host interactions, curbing infection. These outcomes suggest utilizing molecular recognition for vaccine and therapeutic development can effectively control COVID-19 spread. Nonetheless, these studies lack atomic-scale evidence of the multi-spike protein variant blockade of ACE2. Further research is necessary to understand these interactions' molecular mechanisms and advance treatments.

Molecular recognition entails one molecule (guest) recognizing another (host) via structure-specific, highly selective complex formation [7]. While challenging to directly explore experimentally, numerical simulations offer an alternative. Molecular dynamics simulations with biomolecule force fields (CHARMM, AMBER, OPLS-AA, GROMOS, etc.) elucidate atomic-scale guest-host interactions. This mechanism is vital in biological systems involving receptor-ligand, antigen-antibody, and other complexes with high shape complementarity. For example, Chakraborty analyzed COVID-19 genomes, identifying RBD variants with enhanced ACE2 binding affinity [8]. Similarly, Socher detailed the L452R mutation's hydrogen bond role in the delta variant's RBD-ACE2 interaction [9], indicating that the N501Y mutation increases the alpha and omicron variant's RBD-ACE2 binding energy. Atomistic simulations by Lupala revealed marginally stronger Omicron RBD-ACE2 interactions than the wild type [10]. Pitsillou found Delta and Omicron exhibit stronger ACE2 affinities [11]. Costa's work indicated Omicron has the strongest ACE2 binding [12]. Mutations influenced SARS-CoV-2 RBD-ACE2 interaction dynamics. The all-atom model used in the above studies has brought some critical understanding of spike protein/ACE2 interactions.

Although all-atom molecular dynamics simulations can capture detailed dynamics, they are limited to shorter timescales, further leading to the cost-prohibitive simulation on larger systems. Like the MARTINI model, coarse-grained (CG) models offer practicality in studying large-scale viral processes. The MARTINI CG force field incorporates binding free energy from all-atom models, capturing the structural evolution. Wang used MARTINI CG simulations for SARS-CoV and SARS-CoV-2 envelope organization analysis [13]. Ma employed MARTINI CGMD simulations to study SARS-CoV-2 RBD-human ACE2 interaction [14]. This study used MARTINI CGMD simulations for SARS-CoV-2 variants' binding mechanisms to ACE2.

While experimental studies like ACE2-NPs, GB-1, and IgYs demonstrate molecular recognition's potential for innovative SARS-CoV-2 treatment strategies, they lack in-depth explanations of the binding mechanisms at the atomic scale. Computational modeling can provide insights into spike protein variant interactions with ACE2 to advance novel vaccines and therapeutics. For example, all-atom molecular dynamics simulations have revealed Delta and Omicron RBD mutations can strengthen ACE2 affinity through conformational and electrostatic changes [8–12]. However, all-atom models are limited by short timescales. MARTINI coarse-grained models offer an alternative to studying spike-ACE2 binding kinetics through extensive simulations. While the MARTINI coarse-grained model provides enhanced conformational sampling efficiency, the simplified representation still presents approximations in capturing fine-grained atomistic interaction energies. The general trends and patterns in variant affinities are likely robust, but the precise binding free energies should be considered approximate estimates rather than exact quantities. This study employs MARTINI and nudged elastic band (NEB) calculations to elucidate residue-level spike mutation effects on ACE2 binding energetics and kinetics. The NEB method finds minimum free energy pathways and transition states for conformational molecule changes. The initial and final states are specified, and then intermediate images are created to connect them into a pathway, which is iteratively refined to determine the smoothest route. It reveals energy barrier shapes critical for binding and unbinding. Quantifying mechanisms underlying SARS-CoV-2 infectivity will aid in the rational design of vaccines and drugs targeting emerging viral strains. Molecular modeling is vital for tackling COVID-19 by enhancing understanding of coronavirus spike-ACE2 recognition at the atomic scale. Full spike protein sequences mimic experimental conditions, departing from RBD-focused all-atom models. The MARTINI CG force field and polarized water model in 200 ns simulations allow for investigating key SARS-CoV-2 residues' interaction with ACE2. NEB calculations determine atomic configurations and binding energy barrier heights. This study provides insights into spike protein-ACE2 interaction energy barriers, aiding therapeutic strategy development, and can offer a framework to predict mutation impacts on binding phenotypes for potential future outbreak variants.

2. Simulation model

The coarse-grained model groups multiple atoms into a bead-like unit to simplify molecular systems and enable the simulation of larger processes over longer timescales. These models capture overall dynamics and long-range interactions while smoothing out chemical details. The MARTINI force field specifically maps roughly four heavy atoms into one coarse-grained particle based on chemistry. Two Python scripts, developed by de Jong and colleagues, were employed to generate MARTINI CG models based on the corresponding all-atom (AA) models [15]. The sequence information for the wild type, Delta, and Omicron variants was extracted from the Protein Data Bank (PDB) database using the PDB IDs, 7DDN [16], 7W92 [17], and 7WVN [18], respectively. The AA structures of these three spike-ACE2 complexes were obtained by submitting three spike protein and ACE2 sequences to the SWISS-MODEL web server [19] to generate these three spike-ACE2 complex models based on the variants' and ACE2 sequences and the experimental binding orientations of three spike-ACE2 complexes as templates. The predicted all-atom wild type, Delta, and Omicron variant spike

protein-ACE2 complexes were employed using the SWISS-MODEL web server for further coarse-graining. Fig. 1(a) depicts the ribbon model of the wild-type spike protein-ACE2 complex, highlighting the local secondary structures such as alpha helices, beta sheets, and loops. The spike protein is colored in green, while ACE2 is colored in red. The spike protein of SARS-CoV-2 consists of two functional domains known as S1 and S2. The S1 domain binds to the host receptor, angiotensin-converting enzyme 2 (ACE2), initiating the viral entry process. Within the S1 domain, there are further subdivisions, including the receptor-binding domain (RBD) and the N-terminal domain (NTD). The S2 domain facilitates membrane fusion, allowing the viral genome to enter the host cell. The corresponding AA structure of the wild-type spike protein-ACE2 complex, consisting of 13,677 atoms, is shown in Fig. 1(b). In Fig. 1(c), the corresponding MARTINI CG model of the complex is presented, represented by 2499 beads for the wild-type spike protein and 1375 beads for ACE2. We opted to study the binding of a single spike protomer instead of the entire trimeric structure. Several factors drove this choice: Firstly, examining a single protomer in combination with ACE2 allows for a more straightforward and less complex computational analysis. This approach helps understand the specific binding interactions and kinetics at the residue level, which individual spike mutations can influence. Studying multiple protomers simultaneously could potentially hide these important atomistic details. Secondly, the identical trimeric structure (homotrimeric symmetry) observed in wild-type protomers suggests that the binding behavior seen in a single protomer-ACE2 interaction likely represents the entire trimer. This is also true for the effects of asymmetric mutations, which affect binding on a protomer-by-protomer basis. Our study primarily aims to uncover the specific binding

(a)

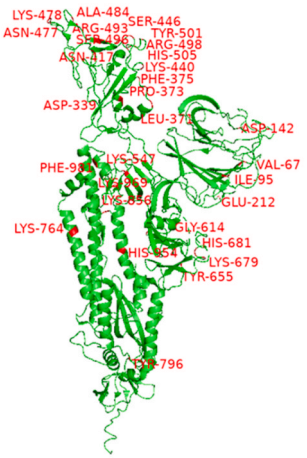

(b)

Fig. 2. Ribbon models of (a) Delta variant and (b) Omicron variant. Delta variant mutations: T19R, G142D, E156G, L452R, T478K, D614G, P681R, and D950 N. Omicron variant mutations: A67V, T95I, Y145D, L212I, G339D, S371L, S373P, S375F, K417 N, N440K, G446S, S477 N, T478K, E484A, Q493R, G496S, Q498R, N501Y, Y505H, T547K, D614G, H655Y, N679K, P681H, N764K, D796Y, N856K, Q954H, N969K, and L981F. Mutation residues and corresponding texts are highlighted in red.

mechanisms affected by spike mutations at the residue level rather than examining the collective effects of the trimer. Concentrating on a single protomer aligns well with our research objectives and methodologies.

Fig. 2(a) and (b) show ribbon models of the Delta and Omicron variants, and the mutation parts and corresponding texts are highlighted in red. Compared to the wild type, the Delta variant exhibits four mutation residues: L452R, T478K, D614G, and P681R. Similarly, the Omicron variant contains the following 30 mutation residues: A67V, T95I, Y145D, L212I, G339D, S371L, S373P, S375F, K417 N, N440K, G446S, S477 N, T478K, E484A, Q493R, G496S, Q498R, N501Y, Y505H, T547K, D614G, H655Y, N679K, P681H, N764K, D796Y, N856K, Q954H, N969K, and L981F, encompassing fifteen mutations within the RBD and the other fifteen in NTD and S2.

To construct the CGMD simulation system, each spike protein variant (or wild type) and ACE2 complex was first placed in a simulation box. The system randomly added water molecules until the density approached 1 g/cm^3. Anions were randomly inserted to ensure system neutrality. The spike protein-ACE2 complexes underwent an equilibration process for 1.0 ns under the NVT ensemble. Subsequently, the NPT MD at 310 K and 0 Pa for 200 ns was carried out using a Berendsen barostat and rescaling thermostat. This timeframe is significant as it exceeds the typical duration of most AA spike-ACE2 simulations found in the existing literature by order of magnitude, offering a more extensive range of conformational sampling. The detailed CGMD simulation information of wild type, Delta, and Omicron variants with ACE2 are summarized in Table 1. For the MARTINI CG model, the Lennard-Jones potential smoothly transitioned to zero between 9 Å and the cutoff distance of 12 Å. Similarly, the Coulombic potential smoothly transitioned to zero between 0 Å and the cutoff distance of 12 Å. All molecular simulations, including the NEB method and MD simulations, were conducted using the Large-scale Atomic/Molecular Massively Parallel Simulator (LAMMPS) package, employing the MARTINI force field (version 2.6P). Molecular structures were visualized and post-processed using OVITO (version 3.5.2) [20]. The binding energy, G_{BE}, is calculated using Eq. (1):

$$G_{BE} = G_{spike/ACE2} - G_{spike} - G_{ACE2} \tag{1}$$

The potential energies of the aqueous systems containing the spike/ACE2 complex, spike protein, and ACE2 are represented by $G_{spike/ACE2}$, G_{spike}, and G_{ACE2}, respectively.

Because the dynamics of the spike protein-ACE2 binding process occur on the time scale of microseconds, it is also too expensive to study it using the molecular dynamics simulation using the MARTINI model. This is because many water beads with spike protein and ACE2 should be used in the simulation. Therefore, the NEB method based on the MARTINI force field was used to find the minimum energy pathway (MEP) and the activation barriers of the spike protein and ACE2 binding process using LAMMPS. The spike protein and ACE2 binding pathway was first mapped using ten frames. In the NEB calculation, intermediate states of spike protein and ACE2 in the water environment are distributed along the reaction coordinate from the known initial state to the final state. Images are coupled with elastic forces, and each intermediate state is fully relaxed in the hyperspace perpendicular to the reaction path. The general NEB method was used to initially determine the MEP with images linearly interpolating between the known initial and final states. Then, the climbing image nudged elastic band (CI-NEB) method was adopted to find the transition state structure of forming the spike protein-ACE2 complex at the saddle point. The system after the NPT MD for 200 ns was used as the initial state of the NEB calculation. For constructing the final state and the intermediate state, the steered molecular dynamics (SMD) [21] was used to simulate the pulling process of spike protein from ACE2, which includes the conformational change along the assumed reaction pathway corresponding to the inverse process of spike protein binding to ACE2.

3. Result and discussion

The value of root mean square deviation (RMSD) is a metric originally used to assess differences between the structures of biological molecules. It is commonly employed to compare the differences between two or more structures of biomolecules [22,23]. To examine the stability of the spike protein as it binds to ACE2, RMSD plots based on trajectory files for the total 200 ns equilibrium simulation were shown in Fig. 3(a)-(c) for wild, Delta, and Omicron, in which the configurations at 0 ns are used as the reference ones for the RMSD calculation. Accordingly, these RMSD plots can measure the differences between the spike protein structure during the simulation and its initial state. The s-protein/ACE2 binding energies during the 200 ns simulation are also shown in Fig. 3(a)–(c) for wild, Delta, and Omicron, respectively. For the wild-type spike protein in Fig. 3(a), the RMSD values during the 200 ns equilibrium

Table 1
Simulation details for CGMD using MARTINI models of wild type, Delta, and Omicron.

Simulation settings	Wild type	Delta	Omicron
Density (initial setting before NPT)	1.00 g/cm^2	1.00 g/cm^2	1.00 g/cm^2
Simulation box (l_x* l_y* l_z)	189.7 Å* 158.21 Å* 247.77 Å	181.80 Å* 159.03 Å* 242.96 Å	173.91 Å* 159.86 Å* 238.15 Å
Dielectric constant	2.5	2.5	2.5
Time step size	10.0 fs	10.0 fs	10.0 fs
Temperature	310 K	310 K	310 K
Pressure	1 atm	1 atm	1 atm
Spike protein	2499 beads	2496 beads	2491 beads
ACE2	1375 beads	1375 beads	1375 beads
Polarized water beads	185549 beads	135086 beads	164414 beads
Cation (Qd type)	26 beads	27 beads	27 beads

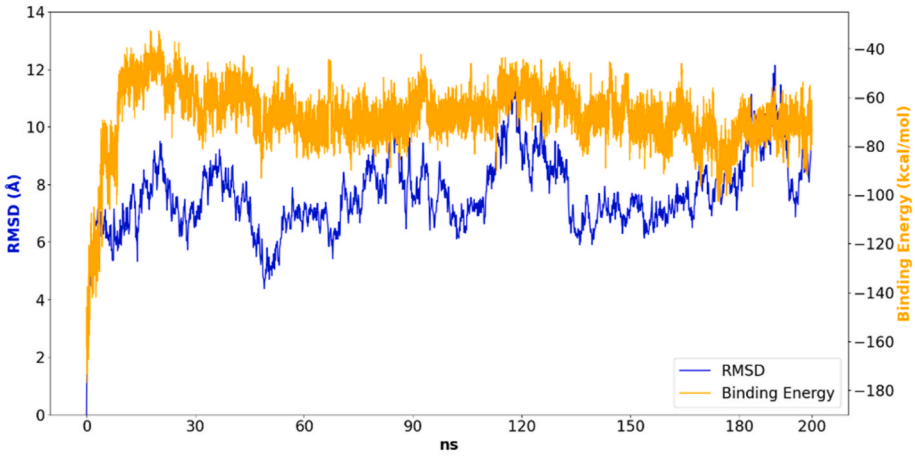

(a)

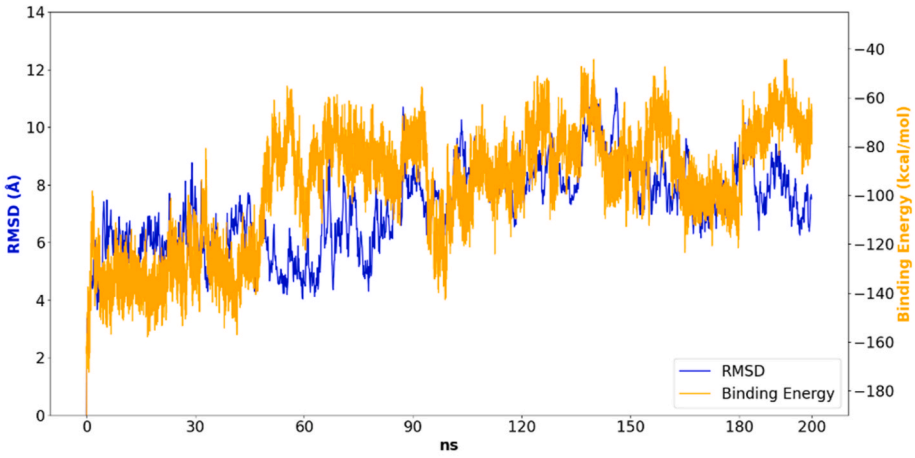

(b)

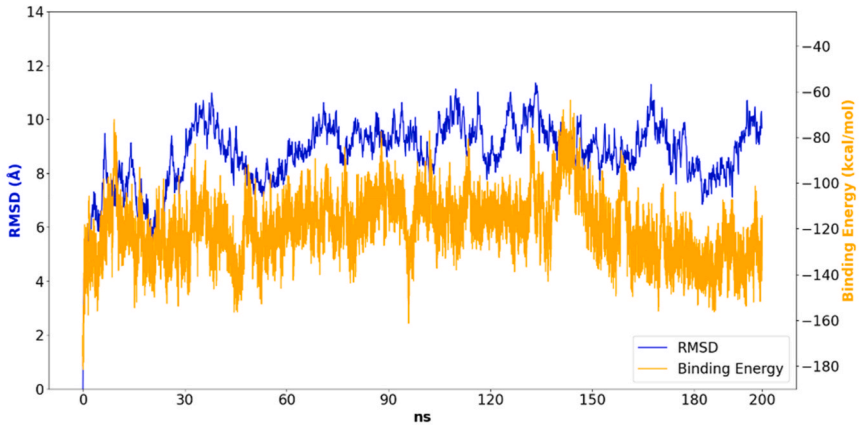

(c)

Fig. 3. The root mean square deviation (RMSD) and binding energy profiles of (a) Wild, (a) Delta, and (c) Omicron for 200 ns equilibrium.

exhibit fluctuations until reaching a stable value around 120 ns. The average RMSD value of the last 50 ns for the wild-type spike protein during the 200 ns equilibrium was 7.66 ± 1.26 Å. In Fig. 3(b), the Delta RMSD values are observed to exhibit fluctuations, stabilizing around a constant value after 120 ns of simulation. The average RMSD value over the last 50 ns of the 200 ns equilibrium period is 7.19 ± 1.51 Å. In Fig. 3(c), the Omicron variant spike protein reaches stability and exhibited fluctuations around a constant value after 60 ns during the 200 ns equilibrium, with an average RMSD value of 8.76 ± 1.16 Å for the last 50 ns. The RMSD values of wild type, Delta, and Omicron reveal all have reached stability in the equilibrium of 200 ns.

Table 2 presents the average binding energy values concerning the interaction between the s-protein and ACE2 and the average RMSD values about the final 50 ns of a 200 ns CGMD simulation. The binding energy values presented in Table 2 provide an overview of the relative stability and affinity between the spike protein variants and the ACE2 receptor. Notably, the Omicron variant demonstrates the strongest overall binding energy at −128.35 ± 10.91 kcal/mol, followed by Delta at −82.78 ± 8.84 kcal/mol, and lastly, the wild type at −73.26 ± 7.46 kcal/mol. This quantitatively confirms that the mutations in the Delta and Omicron variants enhance the spike protein's binding affinity for ACE2 compared to the wild type, as also shown through MD simulations and MM-GBSA binding affinity calculations in studies of Carter et al. [24] and Sang et al. [25]. The increased binding energy of the Omicron variant compared to the wild type likely stems from the optimized electrostatic contacts and hydrogen bonding conferred by mutations like Q493R and Q498R, as described in studies of Philip et al. [26], Carter et al. [24], Sang et al. [25], and Nguyen et al. [27]. The mutations in Delta and Omicron variants appear to fine-tune the spike protein confirmation, allowing tighter binding to ACE2 through conformational and binding affinity changes. In Nguyen's study [27], they explored the binding affinity of the Omicron variant spike protein to the ACE2 receptor using MD simulations and MM-PBSA binding free energy calculations. Their study primarily compares the binding of the Omicron variant RBD to the wild-type RBD with ACE2. It was discovered that the Omicron RBD binds more tightly to human cells than the wild-type, as indicated by its lower binding free energy to ACE2. This enhanced binding affinity of the Omicron variant is primarily due to increased electrostatic interactions. The Omicron RBD's more positive charge significantly strengthens its interaction with the negatively charged ACE2 receptor. Key mutations in the Omicron RBD, particularly N440K, T478K, E484A, Q493R, and Q498R, are identified as major contributors to this improved binding. Verkhivker's study [28] focuses on the binding affinity between the Omicron variant spike protein and the ACE2 receptor using MD simulations and binding free energy calculations of the interaction of the Omicron RBD with ACE2. Results from these computational methods suggest that the Omicron RBD binds with a higher affinity to the ACE2 receptor compared to the wild-type spike protein. This increase in binding affinity is primarily attributed to enhanced electrostatic interactions facilitated by key mutations in the Omicron RBD. Notably, mutations such as Q493R, Q498R, G496S, and N501Y introduce favorable contacts with negatively charged residues on ACE2, thereby strengthening the binding. A related study by Zheng [29] investigated the Omicron variant's RBD of the SARS-CoV-2 spike protein, focusing on its mechanical stability and ACE2 binding ability compared to the wild-type. Using atomic force microscopy, it was found that the Omicron RBD has a 20% higher mechanical unfolding force than the wild-type, indicating greater mechanical stability. This was further supported by single-molecule force spectroscopy experiments, which demonstrated that the Omicron RBD-ACE2 complex exhibits a higher binding probability and rupture force than the wild-type, with an average unbinding force of 63 ± 0.54 pN compared to 54 ± 0.77 pN. MD simulations were conducted to understand these findings at a molecular level. The study employed SMD simulations to mimic the atomic force microscopy experiments, showing that the Omicron RBD requires a higher unfolding force than the wild-type. The results of the current study and all previous related studies consistently find, using a mix of computational techniques, that Omicron binds the strongest, followed by Delta, and wild type is the weakest - fully supporting the current presented order of binding strengths. The consistency in overall trends and residue roles likely arises because both methodologies aim to elucidate binding mechanisms and mutation effects despite differing computational techniques. However, it is worth noting the absolute affinities vary substantially between the MARTINI coarse-grained model values (~100 kcal/mol range) and the related AA simulations (~10–60 kcal/mol range). This likely reflects challenges translating between simulation resolutions. Nonetheless, the trends are preserved, building confidence these mutations truly improve spike-ACE2 binding.

Table 3 displays the breakdown of the binding energies involved in the interactions between several RBD binding sites of three spike proteins and the ACE2. These energies are divided into three levels based on their values: weak interactions (greater than −2 kcal/mol), medium interactions (ranging from −5 kcal/mol to −2 kcal/mol), and strong interactions (lower than −5 kcal/mol), abbreviated as W (for Weak), M (for Medium), and S (for Strong). The specific RBD mutation sites with significantly altered interaction behaviors compared to the wild type are highlighted in bold and red font. Several Omicron mutations like Q493R, G496S, and Q498R introduce stronger interactions with ACE2 that are absent in the wild type. Conversely, the K417 N substitution diminishes the strong wild-type RBD-ACE2 interaction at that residue site. For Delta, the L452R and S477 N mutation sites create medium-strength interactions with ACE2, while the corresponding L453 and S477 of the wild type have no interactions with ACE2. The interplay of these residue-specific enhancements and reductions ultimately drives the overall stronger binding energy of Omicron and Delta variants relative to wild type, as presented in Table 2.

In Fig. 4, the proximity of ACE2 beads (shown in green and blue) to four mutant residues - K417 N, Q493R, G496S, and Q498R

Table 2
Average binding energy between spike protein and ACE2 complex and the average RMSD values.

variants	Binding energy (kcal/mol)	RMSD (Å)
Wild type	−73.26 ± 7.46	7.66 ± 1.26 Å
Delta	−82.78 ± 8.84	7.19 ± 1.51 Å
Omicron	−128.35 ± 10.91	8.76 ± 1.16

Table 3
Interaction Energy (kcal/mol) between RBD Residues (Wild Type, Delta Variant, and Omicron Variant) and ACE2, Categorized as Weak (>−2 kcal/mol), Medium (−5 kcal/mol to −2 kcal/mol), or Strong (<−5 kcal/mol). Residue interaction extents with ACE2: W (Weak), M (Medium), and S (Strong). The RBD mutation residues with significant interaction changes concerning those of wild type are highlighted in red and bold.

Wild type		Delta		Omicron	
G339	≈ 0 (W)		≈ 0 (W)	G339D	≈ 0 (W)
S371	≈ 0 (W)		≈ 0 (W)	S371L	≈ 0 (W)
S373	-0.021 (W)		≈ 0 (W)	S373P	≈ 0 (W)
S375	-0.013 (W)		≈ 0 (W)	S375F	-0.06 (W)
K417	-11.77 (S)		-14.99(S)	**K417N**	-0.017 (W)
N440	-0.29 (M)		-0.12 (W)	N440K	≈ 0 (W)
G446	≈ 0 (W)		-0.027 (W)	G446S	-1.02 (W)
L452	≈ 0 (W)	L452R	-0.02 (W)	L452	-0.023 (W)
S477	≈ 0 (W)		-4.88 (M)	S477N	-0.01 (W)
T478	≈ 0 (W)	T478K	-2.02 (M)	T478K	-2.32 (M)
E484	≈ 0(W)		-1.18 (W)	E484A	-0.044 (W)
Q493	-0.40 (W)		-1.55 (W)	**Q493R**	-25.71 (S)
G496	-0.08 (W)		-1.86 (W)	**G496S**	-5.04 (S)
Q498	-0.36 (W)		-0.32 (M)	**Q498R**	-13.53 (S)
N501	-10.65 (S)		-6.36 (S)	N501Y	-10.23 (S)
Y505	-10.56 (S)		-3.81 (M)	Y505H	-7.90 (S)

(depicted by yellow beads) - is depicted within a 12 Å cutoff from the reference mutant residue. Blue beads, associated with the Delta and Omicron variants, denote ACE2 amino beads that exceed the 12 Å cutoff distance from their positions in the wild type. Additionally, the green beads, also tied to the Delta and Omicron variants, mark ACE2 amino beads that simultaneously remain within the 12 Å cutoff distance from their positions in the wild type. The K417 N mutation in Omicron is associated with the loss of a strong wild-type interaction at that position, as the asparagine substitution eliminates a key electrostatic contact between positive-charged K (Lysine) and negative-charged D30 beads of ACE2. This is visually evidenced in Fig. 4 by the absence of any ACE2 beads for the wild-type case near the K417 N site, and only K353 longer than 11 Å from K417 N exists, resulting in a weak interaction. For Q493R in Omicron, the substitution introduces an extended electrostatic interaction with a distant ACE2 residue that would have been inaccessible in the wild type due to steric constraints. The lone blue ACE2 bead shows this new long-range polar contact around 10 Å from Q493R. Similar behavior is seen for G496S, where serine allows a new hydrogen bond interaction with an ACE2 residue approximately 10 Å away at the edge of the cutoff distance. Lastly, the Q498R mutation enables strikingly proximity between arginine and several ACE2 residues under 6 Å away. The multiple nearby green beads indicate that Q498R likely forms intimate electrostatic interactions that would be impossible with the wild-type glutamine. Overall, the distribution of ACE2 beads around the mutated RBD sites demonstrates how the mutations expand the network of contacts by reducing structural constraints in the wild-type complex. The quantitative binding energy differences from Table 2 indicate the Delta and Omicron variants bind more strongly to ACE2 than the wild type. Table 3 and Fig. 4 offer complementary zoomed-in views of how RBD mutations modulate the residue-specific interactions driving the elevated affinity. The reduced steric hindrance and optimized electrostatic contacts conferred by mutations are evidenced through the stronger binding energies in Table 3 and expanded interaction distances in Fig. 4. Some strong wild-type interactions are also maintained in the mutants, as evidenced by conserved ACE2 beads. For example, N501 retains its close ACE2 contacts despite mutating from asparagine to tyrosine across the variants. This indicates certain critical binding hotspots are preserved, even as the mutations modify other interface areas.

In Pascarella's research [30], they found a discernible rise in positive electrostatic potential from the wild type to the Delta variant and the Omicron variant, giving ACE2 features negatively charged surface patches. This infers that the RBD might exhibit a higher positive electrostatic potential, potentially strengthening the interaction affinity between the viral spike protein and ACE2. In Sang's study [25], they conducted MD simulations using GROMACS 2020.6 and the AMBER99SB force field. Their results indicate the Omicron spike protein exhibits enhanced binding affinity to ACE2, primarily due to electrostatic attraction. In the current study, the uncharged Glutamine (Q) (Q493 and Q498) was mutated to positively charged Arginine (R) (Q493R and Q498R). Q498R introduces new interactions with ACE2 residues E37, E39, and R393 and stronger interaction with negatively charged E35, E37, D38, and D355 beads of ACE2, resulting in an increase in binding energy from −0.08 kcal/mol in the wild type to −13.53 kcal/mol. Additionally, Q493R creates numerous new interactions with ACE2 residues K26, T27, F28, E37, K353, and D355 as well as stronger interaction with negatively charged D30, E35, E37, and D355 beads of ACE2, leading to a substantial increase in binding energy from −0.08 kcal/mol in the wild type to −25.71 kcal/mol, making it the highest binding energy on the Omicron RBD. Both Q493R and Q498R mutations benefit from their positive charge, increasing interactions with the negatively charged ACE2 and raising the binding energy. Similar results of G496S can also be seen for the interaction between positively charged G496S and negatively charged E35, E37, and D38 beads of ACE2. Conversely, the K417 N mutation on Omicron, where the positively charged Lysine (K) interacted with negatively charged D30, was mutated to uncharged Asparagine (N), resulting in a reduction of interactions with ACE2, leading to a decrease in binding energy from −11.77 kcal/mol in the wild type to −0.017 kcal/mol.

Fig. 5(a)-(c) illustrate the root mean square fluctuation (RMSF) profiles of the RBDs for the wild type, Delta variant, and Omicron variant, which indicate the dynamics and conformational flexibility of the RBD structures. Higher RMSF values indicate greater vibrational amplitudes of the atoms in the structure, while lower RMSF values suggest relative stability of the particles. The wild type exhibits relatively low RMSF values, indicating a rigid, stable RBD conformation. In contrast, both variants demonstrate higher RMSF values and more fluctuations across the RBD sequence. Specifically, Delta variant shows increased flexibility relative to wild type in several loop regions, including residues 336–347, 364–372, and 393–402. Meanwhile, Omicron displays even greater RMSF increases than Delta, particularly for residues 364–372 and 393–408. The highlighted residues correspond to mutation sites unique to each variant, implying these mutations directly enhance the flexibility of these loops. While the wild-type RBD adopts a rigid state, the mutations in the Delta and Omicron variants appear to confer greater backbone flexibility to key receptor-binding loops. This enhanced conformational freedom likely expands the RBD structural ensemble to modulate binding affinities favorably. As shown in Fig. 4(b) and (c), both Delta and Omicron variants possess the critical residue T478K, displaying a significant RMSF peak higher than that of the wild type. Substituting the electrically neutral Threonine with the positively charged Lysine enhances interactions of RBD with ACE2, resulting in higher activity and flexibility of the T478K residue. In related MD studies [31–33], the RMSF analysis provides critical insights into the structural dynamics of the SARS-CoV-2 variants. Specifically, the RMSF values indicate that the Omicron variant exhibits higher overall flexibility and fluctuations than other variants. This increased flexibility, particularly pronounced in the Omicron variant, is evidenced by its higher RMSF values, suggesting a distinct dynamic behavior that may facilitate its binding to the ACE2 receptor. While all variants show RBD flexibility and stability variations, the Omicron variant stands out with its significantly higher RMSF value, indicating greater flexibility. This characteristic likely contributes to the higher binding affinity of the Omicron variant to the ACE2 receptor, underscoring the complex relationship between structural dynamics and viral binding capabilities.

To explore the wild type, Delta, and Omicron adsorption process near their stable adsorption positions on ACE2 in water environment, the nudged elastic band (NEB) method [34,35] with multiple images implemented by LAMMPS was used to find the minimum energy pathways (MEPs) of wild type, Delta, and Omicron during the binding process in water environment. The steered molecular dynamics (SMD) [21] simulation was used to simulate the pulling process of wild-type, Delta, and Omicron from ACE2, which includes the conformational change along the assumed reaction pathway corresponding to the inverse process of wild-type,

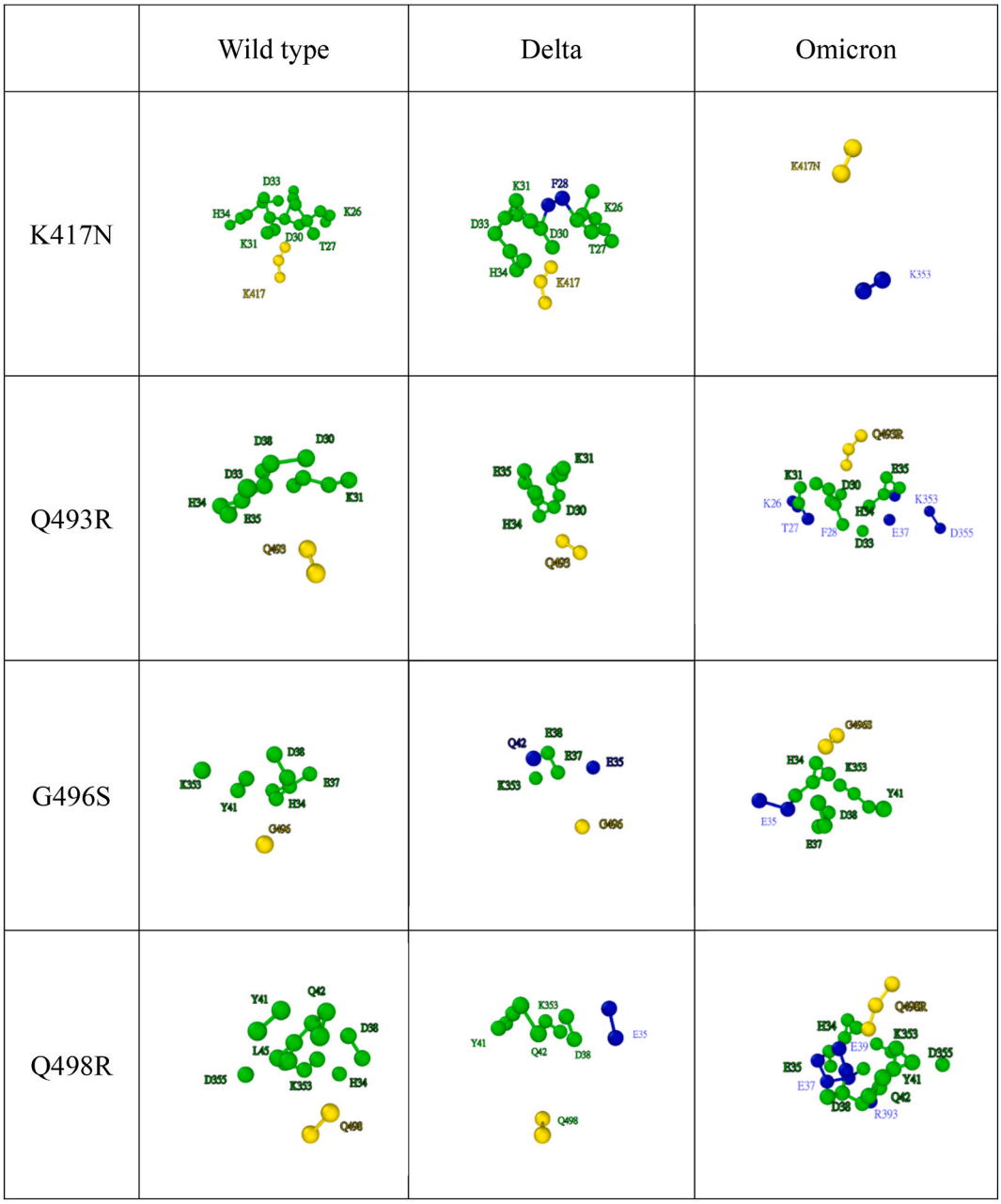

Fig. 4. ACE2 beads (green and blue) within the 12 Å cutoff from key RBD mutation residues (yellow). Blue beads represent ACE2 amino beads beyond the 12 Å cutoff from the wild type residue. See Table 2 for corresponding binding energies.

Delta, and Omicron binding to ACE2. The pulling processes of wild type, Delta, and Omicron from ACE2 by SMD were conducted to prepare reasonable NEB reactant image structures. After the SMD process, the conformational changes of spike proteins and ACE2 were investigated by the variation of RMSD value. The structures of spike protein and ACE2 complexes served as the reference for calculating RMSD values for the structures after SMD. The calculation results for wild-type, Delta, Omicron, and ACE2 are lower than 0.3 Å, indicating no significant conformational change and unfolding occur for wild-type, Delta, Omicron, and ACE2 during the SMD process. Fig. 6 illustrates the MEP and binding energy profiles based on the results of the NEB process for three spike proteins: the wild type, Delta variant, and Omicron variant, each in complex with ACE2. The NEB method provides critical insights into the energy landscape and transition states involved in the spike protein-ACE2 binding process. Due to resource constraints, we initially conducted two independent single SMD runs and NEB calculations for each variant complex using different initial velocity settings for SMD. The conformation of each variant after SMD is very similar to that in the complex, so the MEPs obtained from two independent NEB processes are very close. For the wild-type spike protein in Fig. 6(a), the MEP plot reveals a single main energy barrier with a maximum

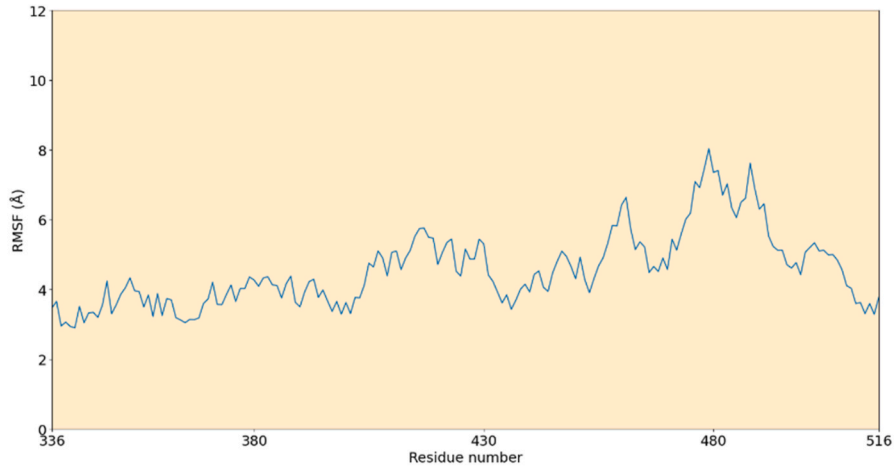

(a)

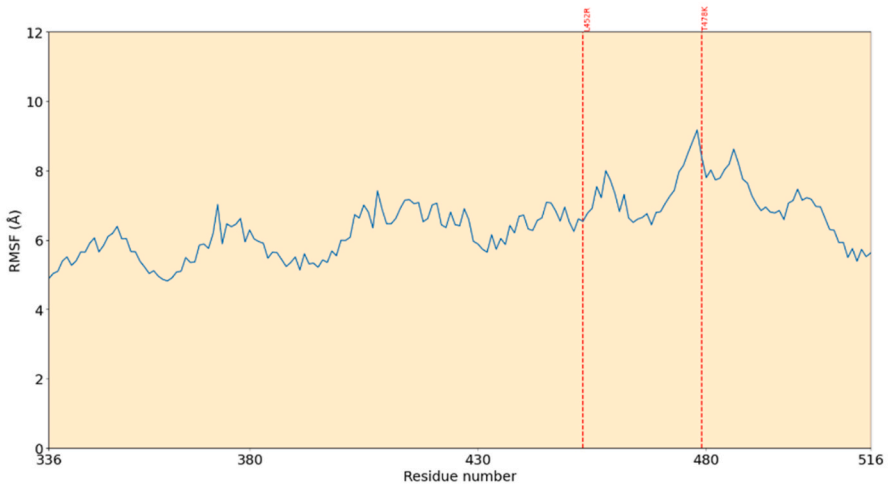

(b)

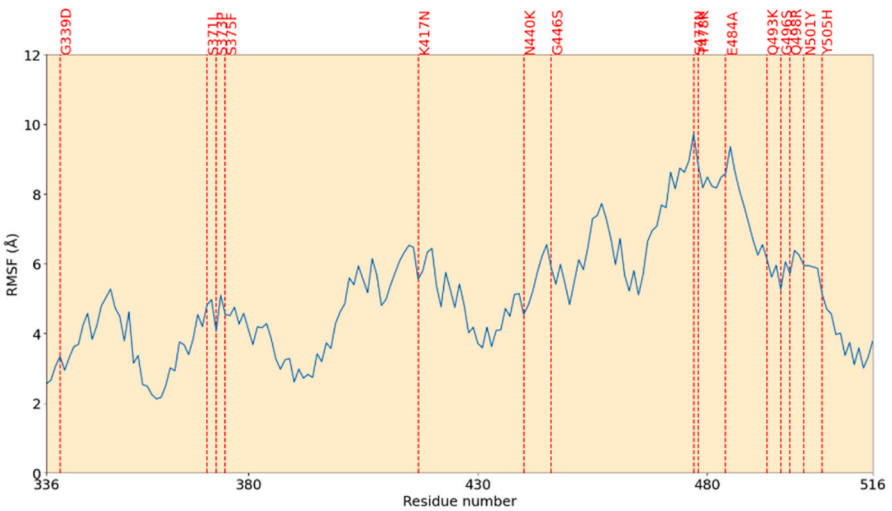

(c)

(caption on next page)

Fig. 5. The root mean square fluctuation (RMSF) profiles of RBD of (a) wild type, (b) (b)Delta variant, and (c) Omicron variant. The vertical dashed lines and the corresponding texts are used to indicate the mutation residues of Delta and Omicron R.

height of approximately 17.87 kcal/mol. This represents the transition state energy along the MEP that must be surmounted for successful binding between the wild-type spike protein and ACE2. In contrast, the Delta variant in Fig. 6(b) displays a lower energy barrier of only 9.21 kcal/mol along its MEP. This indicates the binding process for Delta encounters a minor energetic hurdle to reach the fully bound equilibrium state with ACE2. The mutations in the Delta variant seem to lower the transition state energy compared to the wild type, reducing the kinetic impediment to binding with ACE2. The Omicron variant in Fig. 6(c) exhibits a more complex MEP profile with two clear energy barriers apparent along the MEP. The first barrier reaches 13.36 kcal/mol, while the second barrier is slightly higher at 14.50 kcal/mol. Despite having two energy barriers, their maximum heights are still lower than the wild type at 17.87 kcal/mol. The wild-type spike protein exhibits the highest energy barrier at 17.87 kcal/mol and shows the weakest binding to ACE2. In contrast, the Delta variant displays the lowest barrier at 9.21 kcal/mol and demonstrates stronger binding affinity than the wild type. The Omicron variant has an intermediate dual-barrier profile, with energies lower than the wild type, and shows the most significant binding affinity for ACE2 among the variants. While the Delta variant displayed a lower energy barrier in the NEB analysis, the Omicron variant exhibits a substantially higher binding energy with the ACE2 receptor. Omicron's much greater binding affinity provides a strong driving force that overcomes its slightly higher transition state barriers along the binding pathway, enabling more rapid and stable binding kinetics. Additionally, Omicron's dual transition states give it conformational flexibility to achieve the optimal orientation for ACE2 binding. This combination of high binding energy and adaptive transition state plasticity gives Omicron a key binding advantage over Delta, translating into enhanced viral fusion and entry into host cells.

4. Conclusion

This study utilized CGMD simulations and NEB calculations to investigate the binding mechanisms and energy barriers between the SARS-CoV-2 spike protein variants (wild type, Delta, Omicron) and the human ACE2 receptor. The binding energy results indicate the Omicron variant has the strongest affinity for ACE2 at -128.35 ± 10.91 kcal/mol, followed by the Delta variant at -82.78 ± 8.84 kcal/mol, and the wild type with the weakest at -73.26 ± 7.46 kcal/mol. Mutations in the receptor binding domain of Delta and Omicron optimize electrostatic contacts and reduce steric constraints, enhancing interactions with key ACE2 residues. This is evidenced by strong binding energies at mutation sites absent in the wild type. The NEB binding energy profiles reveal the wild type has the highest transition state barrier at 17.87 kcal/mol, while Delta has the lowest at 9.21 kcal/mol. Despite its slightly higher dual barriers, Omicron's augmented binding driving force enables rapid binding kinetics. The binding energy and NEB results provide a detailed perspective into the molecular factors governing SARS-CoV-2 transmissibility. The Delta and Omicron mutations fine-tune the RBD structure to lower energy barriers and strengthen ACE2 affinity. This combination enhances viral fusion and infectivity compared to the wild type. The study offers insights into mutation effects at the residue level, elucidating mechanisms underlying real-world infectivity trends.

Our study has provided substantial insights that extend beyond the scope of prior computational analyses in several crucial aspects. It reveals a network of binding hotspots within the Omicron variant, mutations of which contribute to increased cumulative affinity, surpassing the singular focus on the well-known N501Y substitution and offering a more holistic view of these mutations' impacts. Furthermore, this study delves into the effects of mutations on the direct spike-ACE2 binding interface and the intricate long-range communication pathways between these proteins, highlighting the mechanisms of allosteric regulation. The study also uncovers the multifaceted role of pivotal Omicron mutations: they intensify local binding interactions while concurrently amplifying the global transmission of allosteric signals, thereby enhancing viral transmissibility. An atomic-level understanding of spike-ACE2 interactions is key for developing treatments and vaccines. This study provides a framework for rational design by quantifying mutation effects on binding energetics and kinetics. The methods here could be applied to emerging concern variants to predict altered infectivity phenotypes rapidly. Molecular modeling is a crucial tool for tackling the ongoing COVID-19 pandemic and potential future coronavirus outbreaks through targeted therapeutics and vaccines.

Data availability statement

The structures (in the lammps data file format) of wild-type, Delta, and Omicron complexes in water can be downloaded at the GitHub repository https://github.com/jushinpon/Sprotein_ACE2.git.

CRediT authorship contribution statement

Shin-Pon Ju: Writing – review & editing, Writing – original draft, Validation, Supervision, Software, Methodology, Investigation, Conceptualization. **Yung-Cheng Yang:** Writing – original draft, Software, Methodology. **Hsing-Yin Chen:** Validation, Methodology, Investigation.

Declaration of competing interest

The authors declare that they have no known competing financial interests or personal relationships that could have appeared to

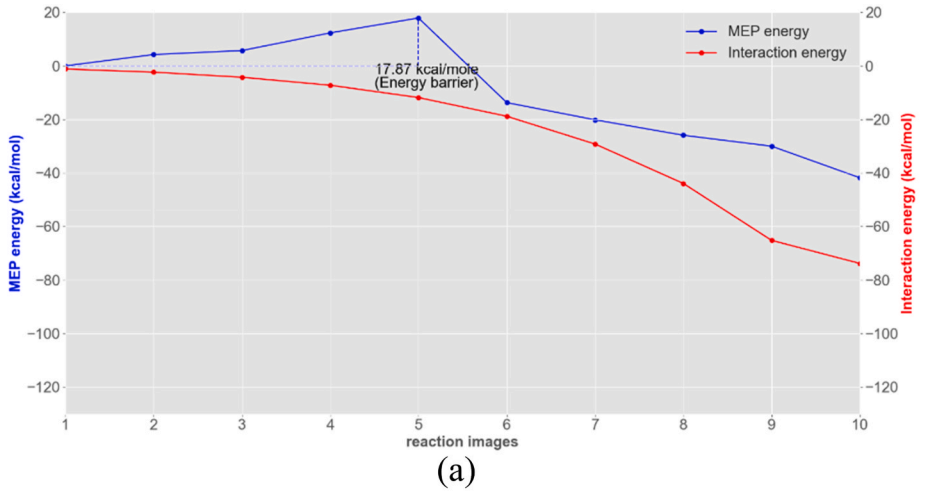

(a)

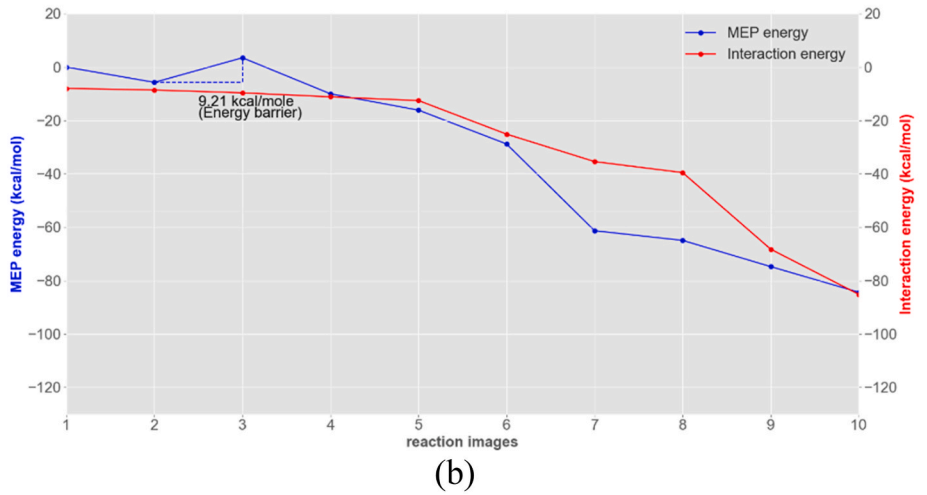

(b)

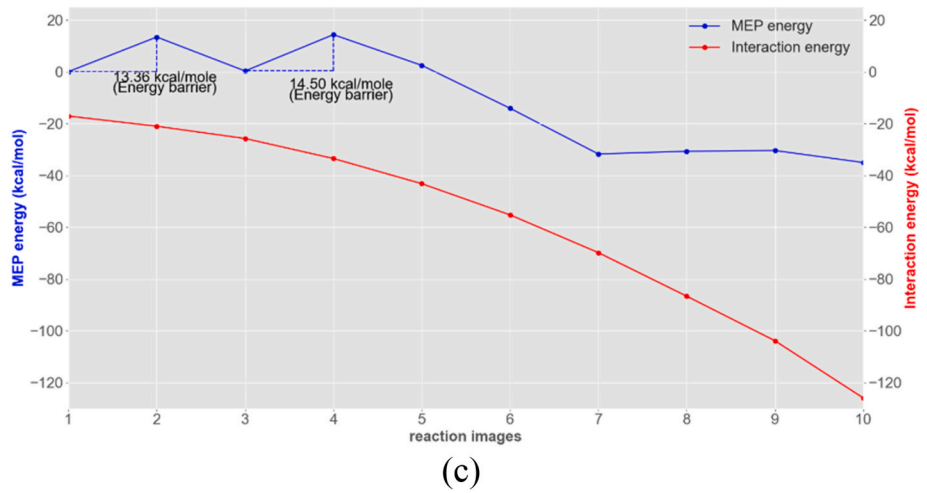

(c)

Fig. 6. Evolution of MEP and binding energy profiles throughout the NEB process for (a) wild type, (b) Delta variant, and (c) Omicron variant in complex with ACE2.

influence the work reported in this paper.

Acknowledgments

The authors would like to thank (1) the Ministry of Science and Technology of Taiwan, under Grant No. 112-2221-E-110-061, and (2) NSYSU-KMU JOINT RESEARCH PROJECT, (#NSYSUKMU 112-P05) for their support on the current study.

References

[1] A. Osterrieder, et al., Economic and social impacts of COVID-19 and public health measures: results from an anonymous online survey in Thailand, Malaysia, the UK, Italy and Slovenia, BMJ Open 11 (7) (2021) e046863.
[2] M. McCallum, et al., Molecular basis of immune evasion by the Delta and Kappa SARS-CoV-2 variants, Science 374 (6575) (2021) 1621–1626.
[3] C. Wang, et al., Membrane nanoparticles derived from ACE2-rich cells block SARS-CoV-2 infection, ACS Nano 15 (4) (2021) 6340–6351.
[4] M.-S. Tsai, et al., Potential inhibitor for blocking binding between ACE2 and SARS-CoV-2 spike protein with mutations, Biomed. Pharmacother. 149 (2022) 112802.
[5] J. Li, et al., Glycyrrhizic acid inhibits SARS-CoV-2 infection by blocking spike protein-mediated cell attachment, Molecules 26 (20) (2021).
[6] S. Wei, et al., Chicken Egg Yolk Antibodies (IgYs) block the binding of multiple SARS-CoV-2 spike protein variants to human ACE2, Int. Immunopharm. 90 (2021) 107172.
[7] J.-M. Lehn, Supramolecular chemistry—scope and perspectives molecules, supermolecules, and molecular devices (nobel lecture), Angew Chem. Int. Ed. Engl. 27 (1) (1988) 89–112.
[8] S. Chakraborty, Evolutionary and structural analysis elucidates mutations on SARS-CoV2 spike protein with altered human ACE2 binding affinity, Biochem. Biophys. Res. Commun. 534 (2021) 374–380.
[9] E. Socher, et al., Molecular dynamics simulations of the delta and omicron SARS-CoV-2 spike - ACE2 complexes reveal distinct changes between both variants, Comput. Struct. Biotechnol. J. 20 (2022) 1168–1176.
[10] C.S. Lupala, et al., Mutations on RBD of SARS-CoV-2 Omicron variant result in stronger binding to human ACE2 receptor, Biochem. Biophys. Res. Commun. 590 (2022) 34–41.
[11] E. Pitsillou, et al., Molecular dynamics simulations highlight the altered binding landscape at the spike-ACE2 interface between the Delta and Omicron variants compared to the SARS-CoV-2 original strain, Comput. Biol. Med. 149 (2022) 106035.
[12] C.H.S. da Costa, et al., Assessment of mutations on RBD in the spike protein of SARS-CoV-2 alpha, delta and omicron variants, Sci. Rep. 12 (1) (2022) 8540.
[13] B. Wang, C. Zhong, D.P. Tieleman, Supramolecular organization of SARS-CoV and SARS-CoV-2 virions revealed by coarse-grained models of intact virus envelopes, J. Chem. Inf. Model. 62 (1) (2022) 176–186.
[14] B. Ma, et al., Evaluation of interactions between SARS-CoV-2 RBD and full-length ACE2 with coarse-grained molecular dynamics simulations, J. Chem. Inf. Model. 62 (4) (2022) 936–944.
[15] D.H. de Jong, et al., Improved parameters for the martini coarse-grained protein force field, J. Chem. Theor. Comput. 9 (1) (2013) 687–697.
[16] C. Zhang, et al., Development and structural basis of a two-MAb cocktail for treating SARS-CoV-2 infections, Nat. Commun. 12 (1) (2021) 264.
[17] Y. Wang, et al., Structural basis for SARS-CoV-2 Delta variant recognition of ACE2 receptor and broadly neutralizing antibodies, Nat. Commun. 13 (1) (2022) 871.
[18] Q. Hong, et al., Molecular basis of receptor binding and antibody neutralization of Omicron, Nature 604 (7906) (2022) 546–552.
[19] A. Waterhouse, et al., SWISS-MODEL: homology modelling of protein structures and complexes, Nucleic Acids Res. 46 (W1) (2018) W296–W303.
[20] A. Stukowski, Visualization and analysis of atomistic simulation data with OVITO–the Open Visualization Tool, Model. Simulat. Mater. Sci. Eng. 18 (1) (2010) 015012.
[21] S. Izrailev, et al., Steered molecular dynamics, in: Computational Molecular Dynamics: Challenges, Methods, Ideas, Springer Berlin Heidelberg, Berlin, Heidelberg, 1999.
[22] B.A. Reva, A.V. Finkelstein, J. Skolnick, What is the probability of a chance prediction of a protein structure with an rmsd of 6 A? Folding Des. 3 (2) (1998) 141–147.
[23] V.N. Maiorov, G.M. Crippen, Significance of root-mean-square deviation in comparing three-dimensional structures of globular proteins, J. Mol. Biol. 235 (2) (1994) 625–634.
[24] C. Carter, J. Airas, C.A. Parish, Atomistic insights into the binding of SARS-CoV-2 spike receptor binding domain with the human ACE2 receptor: the importance of residue 493, J. Mol. Graph. Model. 118 (2023) 108360.
[25] P. Sang, et al., Electrostatic interactions are the primary determinant of the binding affinity of SARS-CoV-2 spike RBD to ACE2: a computational case study of omicron variants, Int. J. Mol. Sci. 23 (2022), https://doi.org/10.3390/ijms232314796.
[26] A.M. Philip, W.S. Ahmed, K.H. Biswas, Reversal of the unique Q493R mutation increases the affinity of Omicron S1-RBD for ACE2, Comput. Struct. Biotechnol. J. 21 (2023) 1966–1977.
[27] H.L. Nguyen, et al., SARS-CoV-2 omicron variant binds to human cells more strongly than the wild type: evidence from molecular dynamics simulation, J. Phys. Chem. B 126 (25) (2022) 4669–4678.
[28] G. Verkhivker, et al., Computer simulations and network-based profiling of binding and allosteric interactions of SARS-CoV-2 spike variant complexes and the host receptor: dissecting the mechanistic effects of the delta and omicron mutations, Int. J. Mol. Sci. 23 (8) (2022).
[29] B. Zheng, et al., S373P mutation stabilizes the receptor-binding domain of the spike protein in omicron and promotes binding, JACS Au 3 (7) (2023) 1902–1910.
[30] S. Pascarella, et al., The electrostatic potential of the Omicron variant spike is higher than in Delta and Delta-plus variants: a hint to higher transmissibility? J. Med. Virol. 94 (4) (2022) 1277–1280.
[31] C.A. Beaudoin, et al., SARS-CoV-2 Omicron subvariant spike N405 unlikely to rapidly deamidate, Biochem. Biophys. Res. Commun. 666 (2023) 61–67.
[32] K. Kodchakorn, P. Kongtawelert, Molecular dynamics study on the strengthening behavior of Delta and Omicron SARS-CoV-2 spike RBD improved receptor-binding affinity, PLoS One 17 (11) (2022) e0277745.
[33] K.A. Idowu, C. Onyenaka, O.A. Olaleye, A computational evaluation of structural stability of omicron and delta mutations of SARS-CoV-2 spike proteins and human ACE-2 interactions, Inform. Med. Unlocked 33 (2022) 101074.
[34] G. Henkelman, B.P. Uberuaga, H. Jónsson, A climbing image nudged elastic band method for finding saddle points and minimum energy paths, J. Chem. Phys. 113 (22) (2000) 9901–9904.
[35] V. Ásgeirsson, et al., Nudged elastic band method for molecular reactions using energy-weighted springs combined with eigenvector following, J. Chem. Theor. Comput. 17 (8) (2021) 4929–4945.